We are Nitinol.™

Structural Determination of Small Amorphous Volumes by Electron Diffraction

Moine, Sinclair, Pelton

Journal of Non-Crystalline Solids 101
pp. 213-222

1988

www.nitinol.com
47533 Westinghouse Drive Fremont, California 94539 t 510.683.2000 f 510.683.2001

Journal of Non-Crystalline Solids 101 (1988) 213–222
North-Holland, Amsterdam

STRUCTURAL DETERMINATION OF SMALL AMORPHOUS VOLUMES BY ELECTRON DIFFRACTION

P. MOINE [a], A.R. PELTON [b] and R. SINCLAIR [c]

[a] *Laboratoire de Metallurgie Physique, Faculté des Sciences, University of Poitiers, 86022 Poitiers, France*
[b] *Department of Materials Science and Engineering, University of Notre Dame, Notre Dame, IN 46556, USA*
[c] *Department of Materials Science and Engineering, Stanford University, Stanford, CA 94305, USA*

Received 22 July 1987

A method is described to obtain structural information from small amorphous volumes by electron diffraction. Microdensitometer traces of electron diffraction patterns are used to produce scattering profiles from which radial distribution functions are derived. This technique is discussed for application for the characterization of amorphous thin films and ion- and electron-irradiated amorphous samples. A specific example is illustrated for sputter-deposited and ion-bombarded $Ni_{56}Ti_{44}$ alloys. The sputtered thin films were additionally characterized by traditional X-ray diffraction procedures. With both diffraction techniques, the first peak maximum in the radial distribution curves occurs at 2.58 Å, whereas the other peak positions are within 2% of each other, Furthermore, the coordination numbers derived from the two methods are in good agreement.

1. Introduction

Techniques for structural characterization of amorphous materials by X-ray and neutron diffraction are well established. In particular, it is straightforward to determine atomic radial distribution functions (RDFs) from diffractometer scans. As with all X-ray and especially neutron methods, a rather large amount of material is necessary to yield a diffraction pattern with a signal adequate for analysis. However, there are many practical instances when only small crystalline volumes are available. This is the case, for example, when the amorphous material is in the form of a very thin film or has been produced locally by ion implantation or high energy electron irradiation. In such circumstances, electron diffraction is extremely valuable since quite intense patterns can be obtained from small scattering volumes.

In principle, RDFs can be calculated from electron scattering data; however, this method is rarely applied for the following reasons. First, the atomic scattering amplitudes for electrons decrease rapidly as the scattering vector, Q, increases. As such, the scattering intensity for large values of Q is very weak. Second, in some conditions, the inelastic scattering intensity may dominate the elastic scattering. Third, multiple scattering cannot be taken into account due to difficulties in accurate calculations. Despite these drawbacks, Fujime [1] described a method based on the assumption that incoherent scattering of an amorphous region is the same as the background intensity of the same region after crystallization. This technique has also been applied with success, after some modifications, by Nandra and Grundy [2] and by the present authors [3].

Previous investigators employed electron diffraction techniques only to analyze thin amorphous films; see, for example, the review by Dove [4]. To our knowledge, however, there have been no previous reports on structural characterization of irradiated amorphous materials. Thus, the purpose of this article is to demonstrate that modern transmission electron microscopes (TEMs) offer unique advantages for the analysis of small noncrystalline regions. It will be shown that important experimental parameters such as coordination numbers and average first-neighbor bond lengths may be

obtained with a good approximation by electron diffraction. The first part of this paper will deal with the formalism and with the theoretical explanation of the experimental procedure that is based on Fujime's method [1]. The second part will describe the experimental details and especially the most commonly encountered critical problems. For the electron-based method to be applied to small scattering volumes, it must be shown that the structural information is equivalent to X-ray based analysis for bulk samples. Therefore, in the third part of this paper an application of this technique to a vapor-deposited amorphous $Ni_{56}Ti_{44}$ thin film will be presented. RDFs are deduced and critically compared after both X-ray and electron diffraction intensity analysis. These thin-film results will then be compared with electron-diffraction generated data from ion-implanted $Ni_{56}Ti_{44}$.

2. Formalism and theoretical procedure

2.1. Formalism

We will follow the same formalism as that used by Wagner [5] in his recent review paper on the structural analysis of amorphous materials. If $\rho(r)$ is the total atomic distribution function, the radial distribution function, $R(r)$, is $4\pi r^2\,\rho(r)$. The integral

$$\int_r^{r+\Delta r} R(r)\,\mathrm{d}r$$

gives the average number of atoms at distances between r and $r+\Delta r$ from a given atom chosen as the origin. The total structure factor (or total interference function) is [6]:

$$I(Q) = \frac{I_N(Q)/N - (\langle f^2\rangle - \langle f\rangle^2)}{\langle f\rangle^2}. \tag{1}$$

The scattering vector, Q, is $4\pi \sin\theta/\lambda$, $I_N(Q)$ is the observable coherent scattering intensity, N is the number of atoms, and f is the electron scattering factor. The quantity $I_N(Q)/N$ is the total, coherently scattered intensity per atom [5]. For a two-component system, $\langle f^2\rangle = x_1 f_1^2 + x_2 f_2^2$ is the mean square scattering factor, and $\langle f\rangle^2 = (x_1 f_1 + x_2 f_2)^2$ is the square of the mean scattering factor. The experimental scattering intensity $I_{OBS}(Q)$ has two contributions:

$$I_{OBS}(Q) = I_N(Q) + I_{incoh}(Q), \tag{2}$$

where $I_N(Q)$ is the coherent scattering intensity and $I_{incoh}(Q)$ is the incoherent intensity.

The Fourier transform of $Q[I(Q)-1]$ (the total reduced structure factor) yields the reduced atomic distribution function, $G(r)$:

$$G(r) = \left[R(r) - 4\pi\rho_0 r^2\right]/r = 2/\pi \int_0^\infty Q[I(Q)-1]\,\sin Qr\,\mathrm{d}Q, \tag{3}$$

where ρ_0 is the average atomic density.

2.2. Electron scattering intensity analysis

In order to obtain the RDF from the experimental data, it is clearly necessary to obtain reliable values of $I(Q)$. The following procedure is adopted in the present study: electron diffraction patterns are obtained in the usual way and the reciprocal space is scaled by using diffraction patterns with known diffraction vectors. This is most easily achieved in the present situation with the use of crystallized material when the initial state is amorphous, or the original crystalline structure in the case of subsequently ion-implanted or electron-irradiated specimens. According to eq. (2), it is necessary to isolate $I_{incoh}(Q)$ from $I_{OBS}(Q)$. In the absence of energy filtering, $I_{incoh}(Q)$ is assumed to be equivalent to the background intensity, $I_{BG}(Q)$, of the same region after crystallization [1] such that

$$I(Q) - 1 = \frac{I_{OBS}(Q) - \alpha I_{BG}(Q) - \beta\langle f^2(Q)\rangle}{\beta\langle f(Q)\rangle^2}. \tag{4}$$

The normalization constant, α, takes into account a possible difference in the density of photographic plates exposed at the same scattered intensity. Figure 1 shows typical microdensitometer traces from amorphous and crystalline films. Of pertinence to the present discussion is the superimposed dotted curve which represents the background intensity, $I_{BG}(Q)$. In order to evaluate α

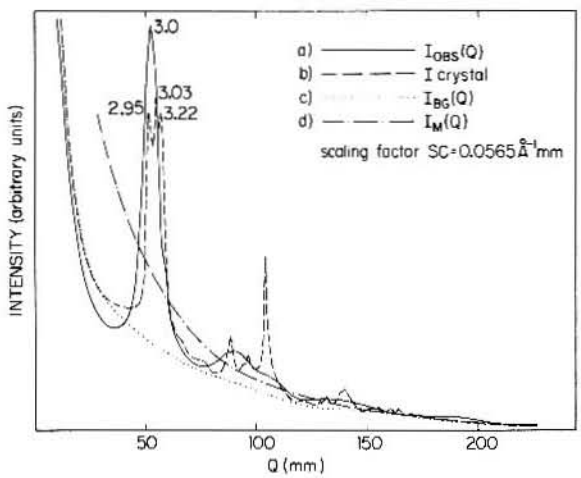

Fig. 1. Microdensitometer traces of amorphous and crystallized scattering patterns of sputtered $Ni_{56}Ti_{44}$. The crystalline pattern, $I_{crystal}$, corresponds to Ni_3Ti, which has a DO_{24} crystal structure. The background intensity, I_{BG}, is suitably drawn to fit $I_{crystal}$. The function, $I_m(Q)$ passes midway through the maxima and minima of $I_{OBS}(Q)$.

and β, a function $I_M(Q)$ is defined as $I_M(Q) = \alpha I_{BG}(Q) + \beta\langle f^2(Q)\rangle$. α and β are adjusted such that $I_M(Q)$ passes midway through the maxima and minima of $I_{OBS}(Q)$, and coincides with $I_{OBS}(Q)$ at large values of Q. This relationship is illustrated in fig. 1 by a dotted-broken line. Equation (4) may then be written as:

$$I(Q) - 1 = \frac{I_{OBS}(Q) - I_M(Q)}{\beta\langle f(Q)\rangle^2}. \tag{5}$$

The absolute zero-intensity level of the photographic negatives (recorded on an unexposed region) cannot be accurately determined. Therefore, to take the background level into account, a constant C is added to the relationship for $I_M(Q)$ such that $I_M(Q) = \alpha I_{BG}(Q) + \beta\langle f^2(Q)\rangle + C$. $I(Q)$ is almost equal to 0 at $Q = 0$ and remains negligible for metallic glasses when Q is less than approximately $Q_1/3$, where Q_1 is the scattering vector of the $I(Q)$ first maximum. Consequently, if ϵ represents a small scattering vector, then

$$I_{OBS}(\epsilon) - \alpha I_{BG}(\epsilon) \cong \beta\{\langle f^2(\epsilon)\rangle - \langle f(\epsilon)\rangle^2\} + C. \tag{6}$$

In general for metallic glasses, and in particular for Ni–Ti alloys, the quantity $\beta\{\langle f^2(\epsilon)\rangle - \langle f(\epsilon)\rangle^2\}$ is negligible when compared to $I_{OBS}(\epsilon)$. Furthermore, C is always a very small constant such that $I_{OBS}(\epsilon - \alpha I_{BG}(\epsilon) \simeq 0$ and $\alpha \simeq I_{OBS}(\epsilon)/I_{BG}(\epsilon)$. α is calculated in this manner for the smallest ϵ scattering vectors of the experiment. β and C are then calculated by a least-squares method from eq. (6). $I_M(Q)$ and $I(Q)$ can then be deduced. Corrections for multiple scattering were not attempted.

To calculate $G(r)$ from $I(Q) - 1$, a damping factor, $\exp(-BQ^2)$, is incorporated in the integral to minimize the influence of the inaccurate values of $I(Q)$ at large Q:

$$G(r) = 2/\pi \int_0^{Q_t} (I(Q) - 1) \exp(-BQ^2) \sin Qr \, dQ. \tag{7}$$

Following conventional practice, B was chosen so that $\exp(-BQ_t^2) = 0.1$. Ripples appear in $G(r)$ at values for r less than the nearest-neighbor distance due to inaccuracies in $I(Q)$ and the termination of the integral Q_t. However, beyond a value of $Q_t = 10$ Å^{-1}, the termination does not significantly affect the RDF, except for ghost maxima at distances $\Delta r \simeq \pm 5\pi/2Q_t$ and $\pm 9\pi/2Q_t$ from the main peak [7].

2.3. Coordination number

In amorphous materials, only the first peak in the RDF is sufficiently well defined to allow an evaluation of the total coordination number of the nearest neighbors. With this proviso, the coordination number is

$$N = \int_0^{r_1} R(r) \, dr,$$

where r_1 corresponds to the first minimum (after the first maximum) of the RDF. Coordination numbers calculated in this manner are generally overestimated; however, this technique does not require any extrapolation method or Gaussians fit to the first RDF peak and it is self-consistent.

3. Experimental procedure

3.1. Specimen preparation

Usual thinning techniques are used to prepare transmission electron microscope specimens. Thus,

in the case of amorphization by ion implantation, two techniques may be used: (1) the surface of a 3-mm diameter disc is amorphized by ion implantation and a TEM sample is prepared by back-thinning from the non-bombarded surface; or (2) an initially crystalline TEM specimen is amorphized in the ion implanter and observed directly in the microscope. Deposited amorphous thin films can be examined either in through-foil or cross-section orientations.

3.2. *Selected area diffraction patterns; scaling procedure*

When the initial state of the specimen is amorphous a set of selected area diffraction patterns (SADPs) is recorded on photographic plates. Typically, a 2–3 μm selected-area aperture is used to define the region from which the diffraction pattern is obtained. The camera length (i.e. "magnification") of these patterns is adjusted so that the scattering vector, Q, reaches about 15 Å^{-1} on the edges of the plate. Proper exposure of the negatives is critical for subsequent analysis of the diffraction rings. Therefore, the illumination conditions are set at a constant intensity level on the screen and exposure times of between 0.25 and 8 s are used. Furthermore, a beam stop is inserted over the forward-scattered reflection to prevent overexposure and to help locate the center of the SADP. The specimen is then crystallized in situ with a heating stage and returned to room temperature. A new set of SADPs of *the same region* is recorded with the *same* experimental conditions as before. The background intensity, $I_{BG}(Q)$, may then be measured as discussed in sect. 2.2.

In the case of ion implantation, reciprocal space may be easily scaled using the thicker areas of the TEM sample where the amorphous layer (typically between 80 and 200 nm thick) can be seen together with the untransformed crystalline structure. A similar situation arises for an amorphous thin film deposited on a known crystalline substrate. For these samples, the SADP will show both the characteristic halo ring of the amorphous film and the reflections due to the crystal [8]. However, when the initial state is amorphous and there is no substrate, the procedure to scale reciprocal space is clearly more involved. It is imperative that the structures of the crystallized products are well-known and therefore, a preliminary study of the crystallization behavior is often necessary.

For amorphization in a high-voltage electron microscope [9,10] the initial state is crystalline and is used as a standard to scale the reciprocal space and also to obtain $I_{BG}(Q)$. Thus, a set of SADPs is recorded before electron irradiation and another set after the amorphization of *the same region in the same conditions*. These can normally be reproduced to within 2%. With known interplanar spacings, independent values of TEM camera length and electron wavelength are unnecessary.

3.3. *SADP intensity recording: microdensitometer traces*

The scattering intensity was measured from microdensitometer traces across the center of the SADPs with a double-beam recording microdensitometer. The size of the light probe on the negative was about 0.2 mm for a first peak width of about 1.5 mm and the average translation speed of the negative is about 0.2 mm/s. For each set of experiments, the scattered intensity was related to the exposure times for the negatives to obtain a self-consistent proportionality. Typical traces from amorphous and crystalline films are shown in fig. 1. Analysis of these traces will be considered in the next section.

4. Application to an amorphous vapor-deposited $Ni_{56}Ti_{44}$ film

4.1. *Specimen preparation*

An intensive investigation was undertaken to study the structures of amorphous Ni–Ti alloys produced by electron irradiation, ion bombardment and vapor deposition. Full results from this study will be presented elsewhere; in the present paper the preceding structural analysis will be applied to a vapor-deposited $Ni_{56}Ti_{44}$ alloy. This material was obtained by planar-magnetron sputtering a three inch Ni–Ti alloy target with

Ar^+ ions. The specific experimental details of the sputtering conditions may be found in ref. [11]. The substrate was a silicon wafer (3 inch diameter) and the temperature of the static substrate during deposition was estimated to be about 200 °C. The 15 μm thick films were physically stripped from the substrate and the overall composition was determined from an electron microprobe analysis.

4.2. Electron scattering

Three-mm-diameter TEM discs were cut from the amorphous films and were thinned to electron transparency by ion milling with Ar^+ ions at 4 kV and a specimen current of 20–30 μA. TEM images at high magnifications (up to approximately 1 000 000x) in both dark-field and high-resolution operational modes failed to reveal any microcrystalline regions. Furthermore, microchemical analysis with an energy-dispersive spectrometer attached to the TEM was used to confirm that the films were chemically homogeneous within ~ 20 nm diameter regions. A set of SADPs were recorded at room temperature (RT) with a Philips EM400 TEM at 120 kV (fig. 2). A camera length of 450 mm was used to provide a maximum scattering vector of about 15 $Å^{-1}$ at the edge of the negatives. The sample was then heated *in situ* to 550 °C for 10 min to crystallize the film. It was subsequently cooled to RT and a new set of SADPs were recorded under the same conditions (fig. 3). All of the negatives from a particular experiment were developed at the same time and following conventional procedures. Figure 1 shows the traces for the amorphous (a) and crystallized states (b) of this film.

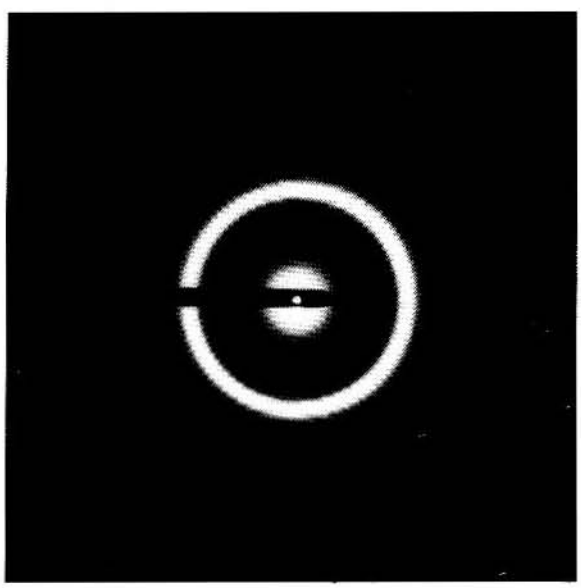

Fig. 2. Electron diffraction pattern of vapor-deposited amorphous $Ni_{56}Ti_{44}$.

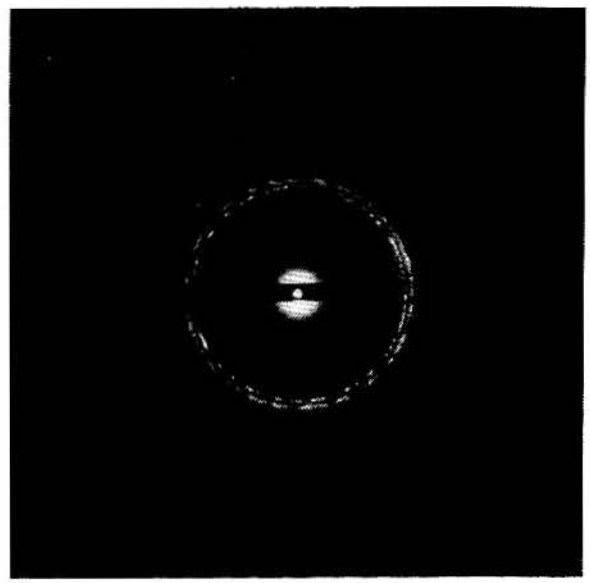

Fig. 3. Electron diffraction pattern of vapor-deposited $Ni_{56}Ti_{44}$ crystallized *in situ* at 550 °C for 10 min.

A structural study of crystallization products under these conditions indicates the formation of disordered phase based on Ni_3Ti (DO_{24} structure) with an overall composition of $Ni_{56}Ti_{44}$ [12,13]. Complementary high-resolution imaging and microchemical analysis studies [14] on similar material confirm the crystal structure and composition of the film. The position of the first three characteristic reflections of Ni_3Ti allows the scaling of the reciprocal space with the scaling constant equal in this case to 5.65×10^{-2} $Å^{-1}$ mm^{-1}.

4.3. X-ray scattering

Reflection X-ray scattering intensity was measured from a diffractometer with MoK_α radiation.

Scans typically covered the scattering angular range corresponding to 0.4 $Å^{-1} < Q < 16$ $Å^{-1}$. Conventional corrections were made to determine the structure factor, $I(Q)$. These corrections include: Compton corrections and Breit–Dirac recoil factor [15]; Fuoss normalization scaling factor (0.900) [16]; and a damping factor ($B = 0.015$) as in the case of electron diffraction.

5. Results

5.1. Electron scattering analysis

The background intensity, $I_{BG}(Q)$, was suitably drawn on the graph of intensity vs. scattering vector in fig. 1(c). The parameters α, β, and C were then determined as described in sect. 2.2. α was estimated to be 0.84 from the ratio $I_{OBS}(Q)/I_{BG}(Q)$ for small Q. β and C were then calculated from the data for 5.5 $Å^{-1} < Q < 10.3$ $Å^{-1}$, and are equal to 3.8 and -1.2 mm, respectively.

The interference function, $I(Q)$, is calculated according to eq. (5) and is shown in fig. 4(a). The numeric values of peak positions are included in the graph. The reduced atomic distribution function, $G(r)$, is then calculated from eq. (8) with a damping factor, $B = 0.015$, and a termination of the integral, $Q_t = 12$ $Å^{-1}$. Finally, the radial distribution function, $R(r) = rG(r) + 4\pi\rho_0 r^2$ is calculated as shown in fig. 5(a). The locations of the peak maxima are also shown in this figure. For comparison, the results of an X-ray scattering analysis from the same sample is presented in the next section.

5.2. X-ray scattering analysis

Figure 6 shows the observed scattering intensity, $I_{OBS}(Q)$, and the total independent scattering of the as-deposited $Ni_{56}Ti_{44}$ thin film. The interference function is calculated similarly to eq. (5) as $I(Q) - 1 = (A - B)/\langle f \rangle^2$, where the functions A and B are illustrated in fig. 6; this interference function is shown in fig. 4(b). The reduced radial distribution function, $G(r)$, is determined from eq. (8) with a termination of $Q_t = 16$ $Å^{-1}$, and the

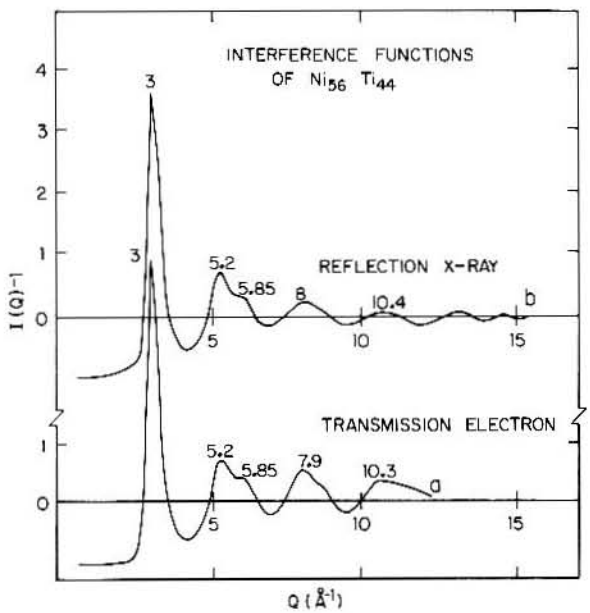

Fig. 4. Interference functions of vapor-deposited $Ni_{56}Ti_{44}$ obtained (a) by electron diffraction analysis, and (b) by X-ray scattering analysis. The peak positions are indicated for comparison.

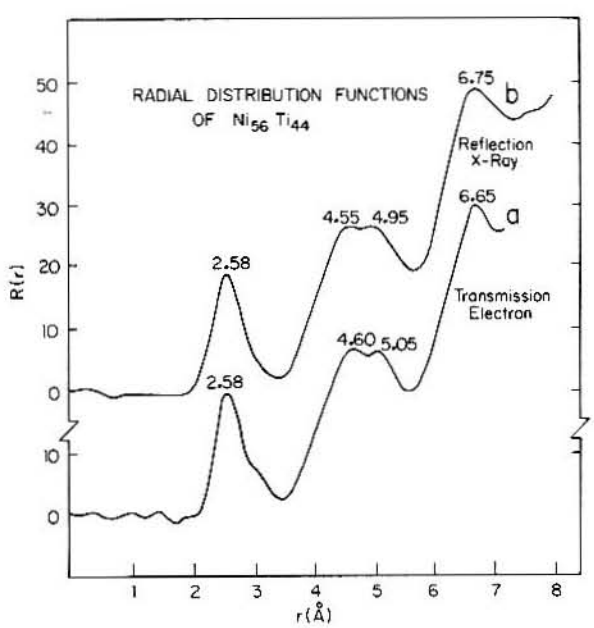

Fig. 5. Radial distribution functions of vapor-deposited $Ni_{56}Ti_{44}$ obtained (a) by electron diffraction analysis, and (b) by X-ray scattering analysis. The peak positions are indicated for comparison.

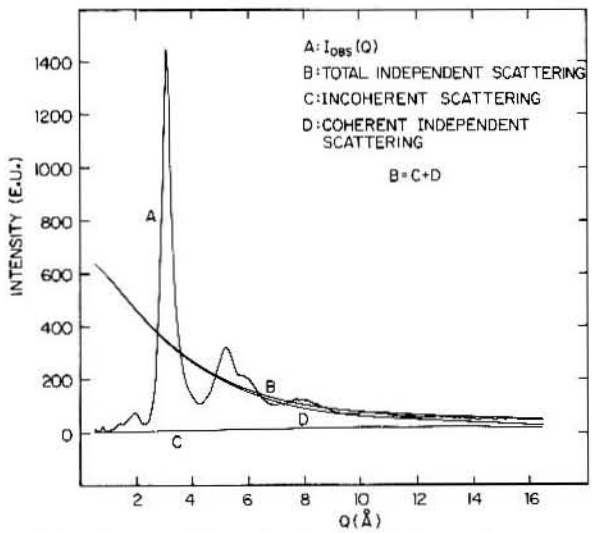

Fig. 6. X-ray scattering intensity profiles of amorphous vapor-deposited $Ni_{56}Ti_{44}$.

corresponding function, $R(r)$ is shown in fig. 5(b).

6. Discussion

The interference functions determined by electron and X-ray scattering analyses from sputtered $Ni_{56}Ti_{44}$ are remarkably similar, as illustrated in fig. 4. Peak locations are the same for $Q < 12$ $Å^{-1}$; specifically, the maximum in the first two peaks occur at 3.0 and 5.2 $Å^{-1}$. Furthermore, the shape and intensity of the first two peaks are in good agreement. In particular, the "shoulder" on the second peak, which is characteristic of metallic glasses [17], is present in both curves. There is also good agreement between RDFs determined from electron and X-ray scattering analysis (fig. 5). The peak locations, intensity and overall shape of the first three peaks are similar. The major difference between the two curves is the presence of ripples that flank the first peak of the electron RDF. However, it is encouraging that the peak positions and hence the average bond lengths are nearly identical in the two curves. For example, from electron diffraction, the first three peaks occur at 2.58, 4.60 (5.05) and 6.65 Å, whereas from X-ray diffraction, these peaks occur at 2.58, 4.55 (4.95) and 6.75 Å. The difference in these data is at most 2% which is within the experimental uncertainties of the electron diffraction method. In addition, first-neighbor coordination numbers were calculated from the data in fig. 5 according to the integral in eq. (9). This analysis yielded values of 13.2 and 13.7 for the X-ray and electron diffraction data, respectively. Although these values are certainly consistent for this alloy, they are somewhat high when compared to previously reported values of 12.1 and 12.8 for liquid-quenched $Ni_{40}Ti_{60}$ [5]. This ~ 10% difference in coordination number between the two alloys may reflect, in part, the difference in composition. More likely, however, this difference is due to the method of calculation. For the present purposes it was deemed unnecessary to employ more sophisticated techniques (such as Gaussian peak-fitting routines) to calculate coordination numbers. It is of interest that the derived coordination number is close to that of the "close-packed" Ni_3Ti crystal structure, but quite different from the eightfold coordination of the $Ni_{50}Ti_{50}$ B2 phase.

Encouraged by these results, this electron diffraction analysis has been extensively used to study the microstructures of amorphous $Ni_xTi_{1-x}(0.3 \leqslant x \leqslant 0.7)$ produced by electron irradiation, ion bombardment and vapor deposition. Although some experiments are still in progress we can illustrate, for comparison, some results related to the amorphous $Ni_{56}Ti_{44}$ produced by ion implantation. Figure 7 shows reduced radial distribution functions, $G(r)$, of amorphous $Ni_{56}Ti_{44}$ produced by vapor deposition and by ion implantation. There are no major differences between these two curves. The coordination number calculated from the ion-implanted sample is 13.9, which is very close to the value of 13.7 from the thin film. The $G(r)$ data are illustrated in this figure rather than $R(r)$ as in fig. 5 so that a comparison may be made with the recent diffraction data from mechanically-alloyed amorphous Ni–Ti alloys [19]. Figure 8 is a reproduction of the reduced radial distribution function of amorphous $Ni_{60}Ti_{40}$ powders prepared by mechanical alloying from the work of Schwarz et al [19]. Specific values of peak positions and coordination number were not tabulated in this reference, which prevents a

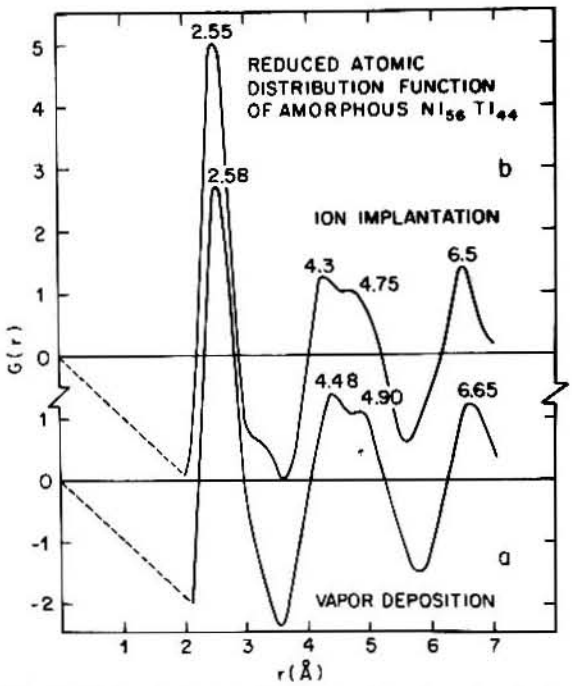

Fig. 7. Reduced atomic distribution functions by electron diffraction analysis from amorphous $Ni_{56}Ti_{44}$ reproduced by (a) vapor deposition and (b) ion implantation.

quantitative comparison to be made with the present data. However, a qualitative comparison between figs. 7 and 8 indicates that there are only minor differences in peak location and peak shape. Schwarz et al. did report that the position of the shoulder on the second peak of $G(r)$ appeared at a fixed position of 5.1 Å for the range of amorphous alloys that they investigated. They attributed this to direct evidence of chemical short range order in the amorphous structure [19]. In fig. 7, the shoulders appear at 4.75 and 4.90 Å for the ion-implanted and vapor-deposited samples, respectively, and are within the expected levels of accuracy for the electron-diffraction method.

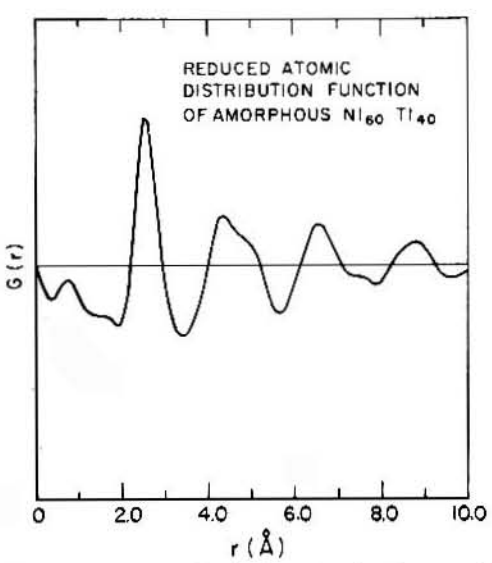

Fig. 8. Reduced atomic distribution function from mechanically-alloyed amorphous $Ni_{60}Ti_{40}$ from Schwartz et al. [19].

The influence of the integral termination, Q_t, has also been investigated when $G(r)$ is calculated from the Fourier transformation of $I(Q)-1$ (eq. 8). For $Q_t < 10$ Å^{-1} the overall shape of the RDF curve is not adversely affected except for more prominent ripples at the low- and high-angle sides of the first peak. The values of coordination numbers and bond lengths remain the same in accord with the discussions in sect. 2.2.

Many of the experimental uncertainties encountered in electron-based investigations of amorphous materials may be minimized by eliminating elastic scattering [4]. A particularly attractive method to achieve this is to filter the scattered electrons through an electron energy loss spectrometer. This method would also give rise to absolute determination of electron intensity. An added benefit is the ability to obtain chemical compositions from the same regions. With this scenario, the diffraction and chemical data could be deconvoluted during the TEM analysis. The feasibility of this method is currently being investigated by the present authors. Some first results using this approach have now been reported for hydrogenated amorphous silicon–carbon alloys [20,21].

The present application clearly demonstrates that electron diffraction in a transmission electron microscope can be effectively used to study amorphous thin films. For $Ni_{56}Ti_{44}$ considered here, the electron-based RDFs are in good agreement with those obtained by X-ray diffraction. Considering the small diffraction volumes which can be employed in TEM, it can be appreciated that the method is extremely useful for those situations where X-ray and neutron diffraction are not feasible, i.e. on the the microscopic level.

Furthermore, the films can be quite thin (e.g. 10 nm) and still produce a significant diffraction signal. This regime is well below the range of conventional X-ray diffraction methods. Additional results on a range of alloy compositions and amorphization techniques (including ion- and electron bombardment) and their relevance to the Ni–Ti system will be presented separately.

7. Conclusion

Transmission electron microscopy techniques have been used to characterize amorphous films of Ni–Ti which are produced by sputter deposition, electron- or ion bombardment. In the latter types of samples, extremely small volumes (~ 0.25–0.5 μm^3) of amorphous material are produced which prevents the use of X-ray and neutron diffraction methods. Therefore, an electron diffraction technique is used to analyze the atomic structure of the films. The basis of this method is the conversion of raw diffraction intensity data from microdensitometer traces of electron diffraction patterns to interference functions. The primary assumption in this analysis is that the contribution from incoherent scattering from the amorphous sample is equivalent to the background intensity of the crystallized material. Although the electron diffraction method is inherently less precise than these traditional diffraction techniques, rather good results may be obtained.

Sputtered films of amorphous $Ni_{56}Ti_{44}$ show the same atomic structure with both electron and X-ray diffraction techniques. There is good agreement between peak positions and coordination numbers from the radial distribution functions obtained by the two methods. However, the coordination numbers are approximately 10% higher than those calculated from liquid-quenched $Ni_{40}Ti_{60}$ alloys. This difference may be due to inaccuracies in the present calculations, or may arise from the different composition.

This electron diffraction method has also been used to analyze the amorphous structure of ion-implanted alloys. In particular, the reduced atomic distribution functions from sputtered and ion-implanted $Ni_{56}Ti_{44}$ are identical. These data are also qualitatively similar to the results from a mechanically-alloyed amorphous $Ni_{60}Ti_{40}$ alloy [19].

Therefore, despite the inherent drawbacks of an electron diffraction analysis, the techniques is quite useful in the study of small volumes of amorphous material. It may be used to obtain quantitative parameters from thin films or as the basis of qualitative comparison.

The authors thank Dr.G. Waychunas for his help with the X-ray diffraction experiments, Mr.M. Noack for his aid in computations and Dr.R.B. Schwartz for the use of fig. 8. This research was supported by the NSF through the Center for Materials Research at Stanford University and in part by a France–USA CNRS–NSF Scientific Cooperation Program (grant number INT 8414029). Support for ARP and PM (summer) was from USDOE at Ames Laboratory which is operated by Iowa State University under contract No. W-7406-Eng-82, supported by the Director of Energy Research, Office of Basic Energy Sciences. Use of the electron microscopy facilities of the Department of Materials Science and Engineering and the Center for Materials Research, Stanford University, is acknowledged.

References

[1] S. Fujime, Jap. J. Appl. Phys. 5 (1966) 764.
[2] S.S. Nandra and P.J. Grundy, J. Phys. F: Metal Phys. 7 (1977) 207.
[3] A.R. Pelton, P. Moine, M.A. Noack and R. Sinclair, Proc. MRS, Vol. 62, eds. L.W. Hobbs, K.H. Westmacott and D.B. Williams (1986) p. 291.
[4] D.B. Dove, in: Physics of Thin Films, eds. G. Hass, M.H. Francombe and R.W. Hoffman (Academic Press, New York, 1973) p. 1.
[5] C.N.J. Wagner, Acta Metall., to be published.
[6] T.E. Faber and J.M. Ziman, Phil. Mag. 11 (1965) 153.
[7] Y. Waseda, The Structure of Non-Crystalline Materials (McGraw-Hill, New York, 1980) p. 34.
[8] P. Moine, J.P. Emery, J.R. Gaboriaud and J. Delafond, Nucl. Instr. and Meth. 207 (1983) 267.
[9] G. Thomas, H. Mori, H. Fujita and R. Sinclair, Scripta Metall. 16 (1982) 589.
[10] A.R. Pelton, Proc. 7th Int. Conf. on HVEM, eds. R.M. Fisher, R. Gronsky and K.H. Westmacott (1983) p. 245.
[11] R.G. Walmsley, Ph.D. Thesis, Stanford Univ. (1981).

[12] P. Moine, A. Naudon, J.J. Kim, A.F. Marshall and D.A. Stevenson, Proc. Int. Conf. NCM3, Grenoble (1985) p. 533.
[13] J.J. Kim, P. Moine and D.A. Stevenson, Scripta Metall. 20 (1986) 243.
[14] A.R. Pelton, A.F. Marshall and Y.S. Lee, Proc. EMSA Meeting 41 (1983) 270.
[15] H.P. Klug and L.E. Alexander, X-Ray Diffraction Procedures (Wiley, New York, 1974) p. 791.
[16] P. Fuoss, Ph.D. Thesis, Stanford Univ. (1980).
[17] G.S. Cargill III, in: Solid State Physics, Vol. 30, eds., H. Ehrenreich, F. Seitz and D. Turnbull (Academic Press, New York, 1975) p. 227.
[18] C.N.J. Wagner, D. Lee, L. Keller, L.E. Tanner and H. Ruppersberg, Proc. 4th Int. Conf. on Rapidly Quenched Metals, eds. T. Masumoto and K. Suzuki, Vol. 1 (Japan Inst. of Metals, Sendai, 1982) p. 331.
[19] R.B. Schwartz, R.R. Petrich and C.K. Saw, J. Non-Cryst. Solids 76 (1985) 281.
[20] D.R. McKenzie, D.J.H. Cockayne and D.M. Duarte, Proc. XI Int. Conf. on Electron Microscopy (1986) p. 539.
[21] A. Sproul, D.R. McKenzie and D.J.H. Cockayne, Phil. Mag. B 54 (1986) 113.